ACS Catalysis

RESEARCH ARTICLE

pubs.acs.org/acscatalysis

Influence of Catalyst Porosity on Ethylene Polymerization

M. P. McDaniel*

Phillips Research Center, Bartlesville, Oklahoma 74006, United States

ABSTRACT: The structure and porosity of Cr/silica catalysts has a strong influence on its activity in ethylene polymerization and on the character of the polymer it produces. In this study, silicas of widely varying physical structure were chosen so that the influence of surface area, pore volume, pore diameter, and coalescence could be independently investigated by monitoring the surface activity, the polymer molecular weight (MW), MW distribution, melt flow, and the amount of long-chain branching (LCB). The results are discussed with respect to (1) fragmentation of the silica during polymerization, and (2) egress of polymer from pores inside the resulting fragments. Pores of narrow diameter were found to inhibit polymer egress, resulting in lower surface participation, which in turn raised the molecular weight. Pores of wide diameter were found to produce relatively constant surface participation and polymer molecular weight, but increased the amount of LCB in the polymer. Variations in MW are seen as a function of the amount of "crowding" within the pore, whereas variations in LCB are seen as a function of the number of active sites within the pore cavity. The physical principles observed from Cr/silica catalysts were found to be independent and additive to other (chemical) influences from Cr/silica catalysts. Moreover, these physical influences apply to other supports and to metallocene catalysts, as well.

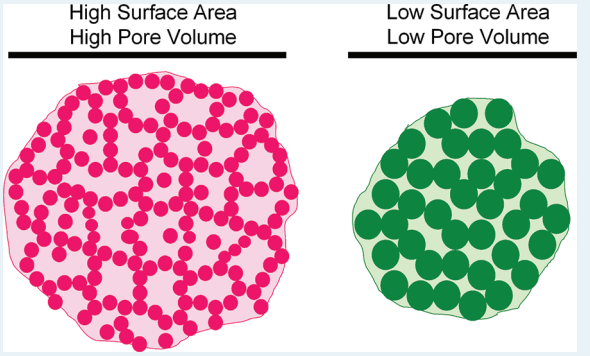

KEYWORDS: ethylene polymerization, chromium catalyst, long-chain branching, polyethylene, catalyst porosity, Phillips catalyst, silica support, silica porosity, metallocene catalysts, polymer molecular weight

INTRODUCTION

The Phillips Cr/silica catalyst is used to manufacture about 40−50% of the world's HDPE supply.[1] From its earliest discovery researchers noted that both its activity and the character of the polymer it produces are related to the porosity of the silica support.[2,3] Some of these trends have been exploited commercially for many years, although without a complete picture of the underlying cause. In this paper, we attempt to set down some of the defining trends and, where possible, to draw insights into the mechanism.

To be active, a polymerization catalyst must rupture shortly after polymerization begins as the pores fill up with polymer, and consequently, the silica structure can be influential to the activity.[1,4−42] This allows monomer access to (and participation by) the entire surface. If the silica is not fragile enough to fragment, it develops limited or no activity. The typical initial 100 μm catalyst particle disintegrates into billions or trillions of fragments, whose dimensions are difficult to measure but have been estimated at 0.1 to 0.01 μm in various studies. In fact, the best Cr/silica catalysts develop activity equal to catalysts made from pyrogenic silicas, which implies that in these cases, fragmentation proceeds until all of the (originally internal) surface can participate.

In highly active Cr/silica catalysts, fragmentation of the structure is generally thought to initiate on the external surface of a macroparticle and along the macro-pores (i.e., those >10 000 Å diameter). However, from the dimension of fragments left, it is clear that the fracturing process must secondarily proceed along mesopores, too. The average silica primary particle is typically 4−10 nm. Therefore, from the fragment dimensions cited above, it is clear that these fragments must measure only a few primary particles across. This explains why nearly all of the (initially internal) surface participates in the polymerization when the structure is optimized.

However, it is also clear that the porosity of the silica influences not only the activity but also the polymer character, and this implies that some polymer is being formed within and "extruded" from shallow mesopores in these fragments. Otherwise, had all the polymer been formed on the exterior of the fragments, its character would not be influenced by catalyst porosity. Therefore, in this study, we have concentrated on the mesoporosity (10−1000 Å). (Macroporosity has also been studied by Hg penetration in the past, but without finding much correlation with polymer properties using polymerization grade silicas. In practice, macroporosity has been varied widely by grinding without much influence on catalyst behavior. It is clearly the mesoporosity that is most important in commercial operations.)

Thus, each catalyst particle of, say, 100−200 μm must fracture into billions or trillions of smaller fragments that then bury

Received: June 9, 2011
Revised: August 25, 2011
Published: August 30, 2011

Scheme 1. Illustration of the Variable Initial Structure of Silica Gels

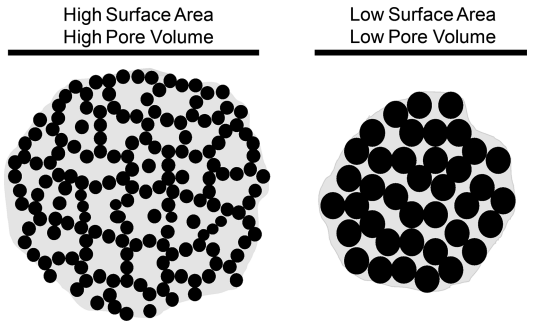

themselves in a coating of polymer. These fragments usually become linked together as polymer chains from one fragment become entangled with chains from neighboring fragments, to produce a large composite polymer particle of, say, 2000 μm diameter. There is some evidence that during this relatively mobile growth and expansion phase, catalyst fragments can sometimes migrate to the exterior, which facilitates monomer access.

Commercial Phillips catalysts are made from gelled silicas. Sodium silicate solution is combined with sulfuric acid to produce an acidic colloidal suspension of silica particles of a few nanometers in diameter. These particles are called "primary particles" because they are the building material of the silica gel network. They remain in suspension because of electrical repulsion until the pH is adjusted upward, causing them to link up into a gel matrix. Where two primary particles collide, surface silanol groups condense to form bonds, or connections, between the two primary particles, holding them together until the entire volume forms a gel matrix.

Scheme 1 illustrates the initial structure of two silica gels. The initial surface area of the gel is determined by the size of these primary particles, and the pore volume is determined by the packing density. In earlier papers,[43−45] we synthesized and tested catalysts incorporating silicas having a wide variety of porosities in an attempt to better understand the polymerization process. In these earlier studies, some polymer properties were studied separately from others because they did not always seem consistent in their responses.

For example, many polymer characteristics are known to depend on catalyst texture, such as flexural and tensile modulus, relaxation and orientation behavior, impact and tear resistance, chemical resistance, molding response, barrier properties, ease of flow, and melt strength. However, all of these can be considered as derivatives of just a few primary molecular features that are controlled by the catalyst. Foremost of these variables are the molecular weight (MW), the molecular weight distribution, and the degree and placement of long- and short-chain branching. It is this latter variable, long-chain branching (LCB), that did not always parallel the trends exhibited by the others, and it was therefore treated separately. In this paper we have tried to summarize and tie together the responses of all these primary variables to catalyst porosity into one comparison and to propose a possible mechanism.

This paper also attempts to model the strength of some silica structures, which is then compared to their observed polymerization behavior. We further note that the act of drying a catalyst hydrogel, which must resist pore shrinkage by surface tension, is another independent measure of the strength of these silicas. The model and the polymerization data were then compared with this shrinkage to gain further understanding of the process.

In the end, we conclude that all of these polymer variables can be tied to two features of the catalyst: (1) The strength of the silica matrix, which determines the extent of disintegration during polymerization and thus the eventual size of the catalyst fragments; and (2) the pore diameter within the fragment from which polymer must extrude, which determines the extent of surface participation and the degree to which polymer chains are restricted during their growth within the pore.

EXPERIMENTAL SECTION

Catalyst Preparation. Both Cr/silica and Cr/silica−titania catalysts are commonly used in commercial operations, and porosity can be varied a great deal for both. For variety, both types were used in this study. Cr/silica−titania tends to produce PE of slightly lower MW and broader MW distribution than Cr/silica.

Silicas were either purchased from W.R. Grace Company or they were made as described below. Chromium acetate was impregnated onto these silicas from methanol to a coverage of 0.4 Cr/nm^2. The catalyst was then dried in a vacuum oven at 100 °C for 12 h.

Cr/silica−titania catalysts were made by cogelation when a solution of chromium sulfate, titanyl sulfate, and sulfuric acid was neutralized by combination with sodium silicate solution, forming a gel. Residual sodium was lowered to 0.03 wt % Na by repeated washing in deionized water. The final hydrogel contained 1 wt % Cr and 3 wt % Ti on a dry weight basis. The hydrogel contained 7 mL of water for each gram of silica it contained. This hydrogel was then dried by various methods as indicated below. Finally, each dried catalyst was sized through a 60 mesh screen.

Cr/aluminophosphate catalysts were made by cogelation of a concentrated solution of aluminum nitrate, dibasic ammonium phosphate, and chromium nitrate. Concentrated ammonium hydroxide was added neutralize the acidity and cause gelation. The gel was then washed several times in alcohol−water solution as noted and dried. Activation was in air at 600 °C for 3 h as described above.

Cr/clay catalysts were made by impregnation of CrO_3 solution into a powdered bentonite, followed by drying and calcination in air for three hours at the indicated temperature.

Metallocene catalysts were made from a solution of 2-(η-5-cyclopentadienyl)-2-(η-5-fluorenyl)hex-5-ene zirconium dichloride in toluene that was then deposited onto sulfate-treated alumina.

Catalyst Calcination. To activate the catalyst, ∼10 g was placed in a 4.5 cm quartz tube fitted with a sintered quartz disk at the bottom. While the catalyst was supported on the disk, dry air was blown up through the disk at a linear velocity of 3.0 cm/s. An electric furnace around the quartz tube was then turned on, and the temperature was raised at a rate of 4 °C/min to 700 °C for Cr/silica and 800 °C for Cr/silica−titania. At that temperature, the silica was allowed to fluidize for three hours in the dry air. Afterward, the catalyst was collected and stored under

dx.doi.org/10.1021/cs2003033 |ACS Catal. 2011, 1, 1394–1407

dry nitrogen, where it was protected from the atmosphere until ready for testing.

Porosimetry. A Quantachrome Autosorb-6 nitrogen pore size distribution instrument was used to determine the surface area, pore volume, and pore volume distribution of the catalysts. The desorption branch was used in pore size distributions.

Polymerization. Polymerization runs were made in a 2.2 L stainless steel reactor equipped with a marine stirrer rotating at 400 rpm. The reactor was surrounded by a stainless steel jacket through which was circulated a stream of hot water, which permitted precise temperature control to within half a degree centigrade, with the help of electronic control instruments. Unless otherwise stated, a small amount (typically 0.05−0.15 g) of the solid catalyst was first charged under nitrogen into the dry reactor. Next, 1.2 L of isobutane liquid was added and the reactor heated to 105 °C. Finally, ethylene was added to the reactor to equal 3.79 MPa (550 psig), which was maintained during the experiment. The slurry was stirred for the specified time, usually about 1 h, and the polymerization was noted by recording the flow of ethylene into the reactor to maintain the set pressure. After the allotted time, the ethylene flow was stopped, and the reactor was slowly depressurized and opened to recover a granular polymer powder. In all cases, the reactor was clean with no indication of any wall scale, coating, or other forms of fouling. The polymer powder was then removed and weighed. Activity was determined from this weight and the measured time.

Gel Permeation Chromatography. Molecular weights and MW distributions were obtained using a Waters 150 CV gel permeation chromatograph with trichlorobenzene (TCB) as the solvent, and a flow rate of 1 mL/min at 140 C. BHT (2,6-di-*tert*-butyl-4-methylphenol) at a concentration of 1.0 g/L was used as a stabilizer in the TCB. An injection volume of 220 μL was used with a nominal polymer concentration of 0.3 g/L (at room temperature). Dissolution of the sample in stabilized TCB was carried out by heating at 160−170 °C for 20 h with occasional, gentle agitation. Two Waters HT-6E columns (7.8 × 300 mm) were used. These columns were calibrated with a broad linear polyethylene standard (Phillips Marlex BHB 5003), for which the molecular weight had been determined.[46]

Rheology Measurements. Rheology measurements were obtained as follows: Samples for viscosity measurements were compression molded at 182 °C for a total of 3 min. The samples were allowed to melt at a relatively low pressure for 1 min and then subjected to a high molding pressure for an additional 2 min. The molded samples were then quenched in a cold (room temperature) press. Disks (2 mm × 25.4 mm diameter) were stamped out of the molded slabs for rheological characterization. Fluff samples were stabilized with 0.1 wt % BHT dispersed in acetone and then vacuum-dried before molding.

Small-strain oscillatory shear measurements were performed on a Rheometrics Inc. rms-800 or ARES rheometer using parallel-plate geometry over an angular frequency range of 0.03−100 rad/s. The test chamber of the rheometer was blanketed in nitrogen to prevent polymer degradation. The rheometer was heated to 190 °C. Upon loading the sample, and after oven thermal equilibration, the specimens were squeezed between the plates to a 1.6 mm thickness, and the excess was trimmed. A total of ∼8 min elapsed between the time the sample was inserted between the plates and the time the frequency sweep was started.

Strains were generally maintained at a single value throughout a frequency sweep, but larger strain values were used for low viscosity samples to maintain a measurable torque. Smaller strain values were used for high viscosity samples to avoid overloading the torque transducer and to keep within the linear viscoelasitc limits of the sample. The instrument automatically reduces the strain at high frequencies if necessary to avoid overloading the torque transducer.

These rheological data were fitted to the Carreau−Yasuda equation to determine zero shear viscosity (η_0), relaxation time (τ), and a measure of the breadth of the relaxation time distribution (CY-a).[47] The long-chain branching (LCB) levels in polymers were calculated using the method of Janzen and Colby[43,45,48] from values of zero shear viscosity and measured values of M_W obtained.

RESULTS AND DISCUSSION

Influence of Pore Volume. The volume occupied by silica hydrogel immediately after gelation does not determine the pore volume (PV) of the final matrix. Rather, the pore volume of the silica is usually determined by the amount of shrinkage that occurs when that hydrogel is then dried. This is because surface tension forms a meniscus that pulls strongly on the pore walls. Shrinkage is especially severe if the pore liquid during drying is water, which has a much higher surface tension than organic liquids.

For example, in one series of experiments, listed in Table 1, samples of a chromia−silica−titania hydrogel were dried in different ways to produce various pore volumes. The hydrogel initially contained 7 mL of water for each gram of silica; that is, it had an initial PV of about 7 mL/g. When the hydrogel was simply dried in an oven at 110 °C, the high surface tension of water pulled on pore walls, shrinking the pores and compressing the gel structure until it was strong enough to withstand the applied force. The dried catalyst, shown as the first entry in Table 1, had a final pore volume of only 0.7 mL/g, indicating a ten-fold shrinkage.

In the second entry in Table 1, the hydrogel was immersed in toluene, whose temperature was raised to the azeotropic boiling point, at which temperature both water and toluene were codistilled off. The condensed distillate was phase-separated, and the toluene phase was continuously returned to the kettle until water stopped coming off, which indicated that all pore water had then been replaced by toluene. The toluene-containing gel was dried at 110 °C. Despite the much lower surface tension of toluene compared with water, this catalyst was still found to have a final pore volume of only 1.0 mL/g. Although the surface tension of toluene (against air) is quite low compared with that of water (also against air), the pores still underwent a high degree of compression. This is because the interfacial tension between pore water and toluene during the distillation process was still quite high.

In the third and fourth entries in Table 1, the pore water was again removed by azeotropic distillation, but in each case, small amounts of isopentyl alcohol were added to the toluene to lower the interfacial tension between the aqueous and toluene phase. This small change raised the pore volumes to 1.3 and 1.7 mL/g.

In the remaining entries in Table 1 samples of hydrogel were also dried by azeotropic distillation with other liquids of varying interfacial and surface tension. The highest pore volume (i.e., the least pore compression) that could be obtained (without resorting to solvents at the critical point) was 3.3 mL/g in this system. This way of drying then became a standard method to make high-PV reference catalysts in further work that is described below.

Table 1. Variation in Pore Volume Caused by Different Methods of Drying Silica Gel [a]

pore liquid (azeotroped, then dried)	pore volume, mL/g	surface area, m^2/g	pore diameter, Å	catalyst activity, kg PE/g Cat/h	surface activity, g PE/m^2/h	melt index, g/10 min
water	0.7	407	56	2.6	6.4	0.12
toluene	1.0	409	80	3.5	8.6	0.32
toluene + 5% isopentyl alcohol	1.3	408	104	3.9	9.6	0.64
toluene + 10% isopentyl alcohol	1.7	411	136	5.1	12.4	1.40
BuOAc	1.8	409	144	6.0	14.6	1.72
BuOAc + 10% isopentyl alcohol	2.0	413	160	6.1	14.8	2.02
BuOAc + 25% isopentyl alcohol	2.2	417	176	6.9	16.5	2.31
EtOAc	2.6	426	208	7.4	17.3	2.53
isopentyl alcohol	3.3	408	264	7.5	18.4	2.88

[a] The pore water in chromia−silica−titania hydrogel was removed by azeotropic distillation while refluxing in various organic solvents.

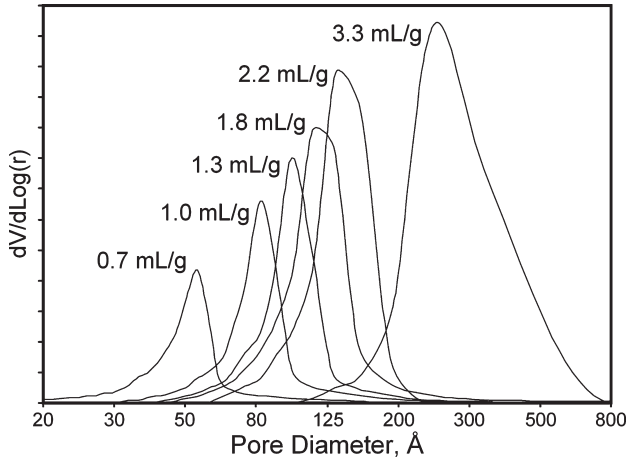

Figure 1. Pore volume distributions of Cr/silica−titania catalysts made by removing the pore water via azeotropic distillation from various organic liquids.

Although the calcined catalysts in Table 1 were chemically identical, both the activity of the catalyst and the polymer produced were strongly influenced by the change in pore volume. Activity increased with rising PV and eventually began to plateau. Melt index, which is a measure of the fluidity of the molten polymer, behaved similarly. High melt index indicates low molecular weight.

As expected, the surface area (SA) in this series of experiments remained constant, at ~410 m^2/g. The average pore diameter (APD) is also listed in Table 1, as calculated from the volume of a theoretical cylindrical pore: APD = 4PV/SA. Thus, the rise in activity and the change in polymer character could also be ascribed to the increasing pore diameter.

Figure 1 shows the pore volume distribution obtained by nitrogen desorption from a similar series of catalysts in which various liquids were used to produce different pore volumes. All of the catalysts produced a single modal curve having a fairly narrow PV distribution. Notice that as the PV (the area under each curve) increases, so does the average pore diameter.

In another series of experiments, depicted in Figure 2, the pore volume was varied in another way. A dry chromia−silica−titania catalyst was obtained that was made like the last entry in Table 1, to have a high pore volume of 3.3 mL/g. Samples of this material were then pressed by a piston in a cylinder at forces varying from zero up to 483 MPa (70 000 psig). With increasing force, the

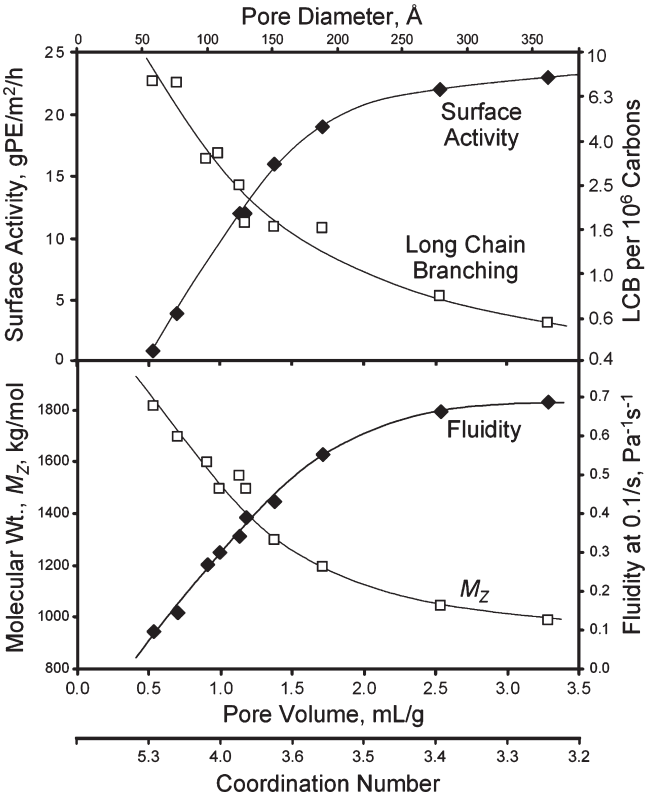

Figure 2. Performance of Cr/silica−titania catalysts having an initial PV of 3.3 mL/g, which had then been compacted in a press at varying pressures to lower the pore volume. Each response is plotted as a function of the pore volume, pore diameter, and the calculated coordination number of each primary particle. Surface area remained constant at ~365 m^2/g.

pore volume of the catalyst dropped so that catalyst having a starting pore volume of 3.3 mL/g was squeezed down to finally about 0.5 mL/g. These catalysts were then calcined and tested for polymerization activity. The variation of surface participation (i.e, activity) and melt index with pore volume in this experiment were almost identical to that in Table 1, indicating that the method of lowering the pore volume was not important in this case. Also plotted in Figure 2 is the *Z*-average molecular weight (M_Z) of the polymer, and the amount of LCB found in it. Molecular weight increased with lower pore volume, and the

dx.doi.org/10.1021/cs2003033 |*ACS Catal.* 2011, 1, 1394–1407

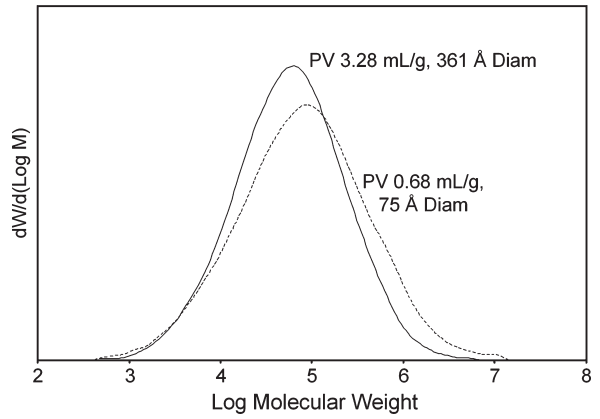

Figure 3. PE molecular weight distributions obtained from high-PV Cr/silica−titania before and after being wet with water and then dried to lower the pore volume.

amount of LCB went up. The *Z*-average MW was chosen for representation here because it is especially sensitive to the higher MW contribution to the MW distribution (see Figures 3, 5, and 7, below).

Once again, the surface area remained relatively constant during this treatment, which indicates that compacting the support, even under the most extreme pressure used here, did not cause enough compression to restrict access by nitrogen. (As pointed out by one reviewer, this could be important in some spectroscopic studies when the catalyst is pressed into a pellet.) Because the surface area was constant, the average pore diameter declined in parallel with the pore volume. Therefore, the average diameter is also shown as one axis at the top of the plot in Figure 2. The pore volume distributions were very similar to those shown in Figure 1, except that the compacted catalysts produced slightly broader peaks.

The change in surface participation with PV in these experiments can be attributed to two influences: (1) polymer (perhaps semimolten) must "extrude" through the pores from the interior of a fragment, and larger pore diameter should facilitate this process; and (2) the PV also controls the strength of the silica matrix, which determines ease of fragmentation during polymerization. Lower PV produces a stronger matrix that can better resist full disintegration, which in turn can lead to larger ultimate fragments. Iler[49] has demonstrated the relationship between pore volume and the average number of neighbors with which each primary particle is in contact. He called this the "coordination number" (CN). For example, in hexagonal close packing, each silica sphere is connected to 12 neighbors (CN = 12) resulting in a pore volume of 0.16 mL/g, whereas in cubic close packing, CN = 6 and PV = 0.42 mL/g, etc. Therefore, we have added the coordination number as another axis in Figure 2.

Just why the polymer character should also change with catalyst pore volume is less intuitive. Sometimes these polymer changes parallel the change in activity, suggesting a common underlying phenomenon. At other times, however, they diverge. These trends are summarized and compared in the Conclusions section, below.

Figure 3 shows still another experiment. In this case, a Cr/silica−titania hydrogel, having a surface area of about 365 m^2/g, was dried by azeotropic distillation in isopentyl alcohol, much like the last entry in Table 1. This produced a pore volume of 3.28 mL/g. A portion of that catalyst was then immersed in liquid water and then redried in an oven. This caused shrinkage so that the final pore volume was only 0.68 mL/g. Both catalysts were then calcined at 800 °C and then tested for polymerization.

As expected, the high-PV catalyst was more active and produced higher fluidity, lower MW, and less long-chain branching. Figure 3 shows how the molecular weight distribution changed with pore volume. Instead of a shift of the entire curve to higher MW, a shoulder developed on the high-MW side of the distribution as the catalyst PV declined. This same behavior was also observed (although not shown) from the experimental series represented by Table 1 and Figure 2.

Influence of Surface Area. An effort was also made to vary the surface area, independently of the pore volume, while maintaining the same silica structure. Silica sols in which the particle size was varied from 7 to 85 nm (SA 325 to 35 m^2/g) were obtained from W.R. Grace (Ludox) and Nyacol (Nexil). These particles remain in suspension until the pH is neutralized, and then they form a hydrogel. Samples of these hydrogels were then impregnated to contain 0.4 Cr/nm^2, and finally, they were dried from different solvents as described above to produce varying pore volumes. Catalysts were then calcined and tested for polymerization activity. Thus, these silicas were made without coalescence or reinforcement (see below). The structure can be considered as an agglomeration of spherical primary particles varying in size.

The results of this experiment are plotted in Figure 4, again as a function of pore volume and coordination number. In the upper left, the surface activity (i.e., the activity expressed per square meter of surface) has been plotted to normalize for the changing surface area. When expressed this way, the activity varies with pore volume, like that in Figure 2. However, for a given PV, vastly differing surface areas still produced similar surface activities, indicating that the size of the primary particle, or its radius of curvature, or the surface area itself, is not critical in determining the activity of that surface in this simple structure.

Polymer character also varied mainly with pore volume, despite large changes in surface area. In Figure 4 the melt flow, molecular weight, and level of long-chain branching are plotted against pore volume, and the resultant lines paralleled those presented above in Figure 2. When these variables were plotted against surface area, no relationship was observed.

These variables were also plotted against the average pore diameter (not shown). A different line was observed for each surface area. This would be expected from the known relationship APD = 4PV/SA if PV is the main variable. This suggests that, in this series at least, pore volume, and not pore diameter, was the main driver.

Figure 5 shows how the molecular weight distribution varied with pore volume for catalyst samples made with the two extremes in surface area (325 and 35 m^2/g). Surface area itself seemed to have no effect. However, for each surface area, one could see the MW distribution changing with pore volume. Once again, declining PV increased the molecular weight not by shifting the entire MW distribution, but by the development of a high-MW shoulder on the main peak. This shoulder became more prominent as the PV dropped so that the MW distribution became bimodal in the most extreme case. This behavior suggests that two kinds of polymer are generated, and the relative amount of each is somehow determined by the catalyst porosity.

Influence of Pore Diameter (Strength Model). These catalysts made from silica sols provide an opportunity to separate the effects of pore volume (which controls the fragility of the

dx.doi.org/10.1021/cs2003033 |*ACS Catal.* 2011, 1, 1394–1407

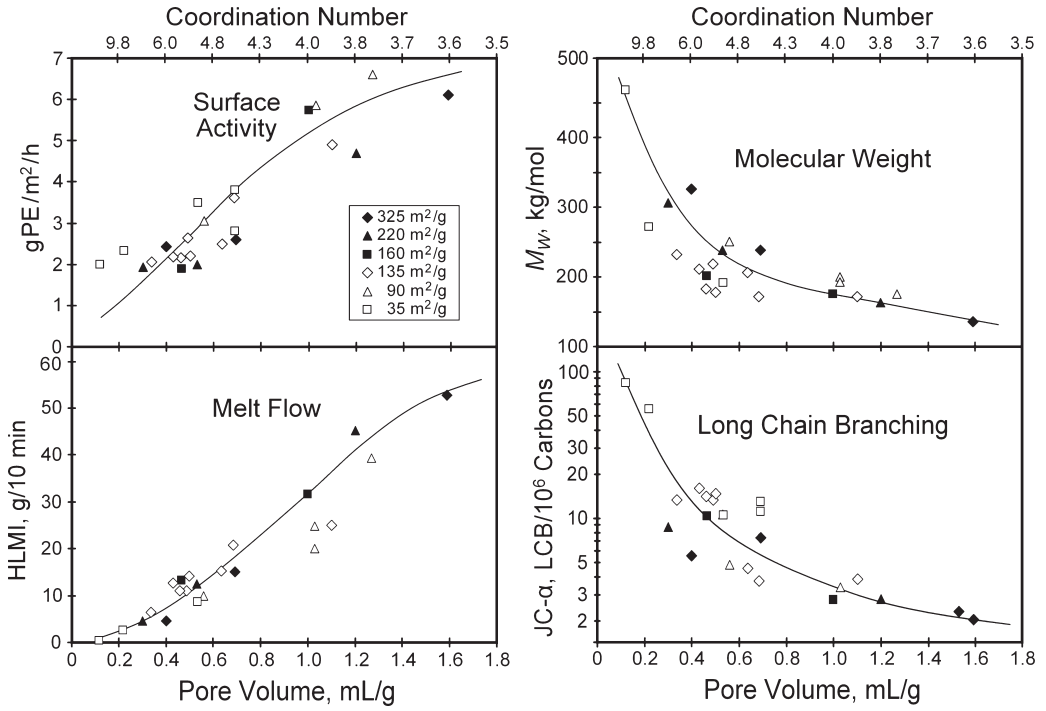

Figure 4. Performance of Cr/silicas made from colloidal particles that were varied in size to produce catalysts of widely differing surface areas but similar structure. Each response is plotted as a function of both pore volume and the calculated coordination number of the average primary particle, but the surface area seemed to matter little.

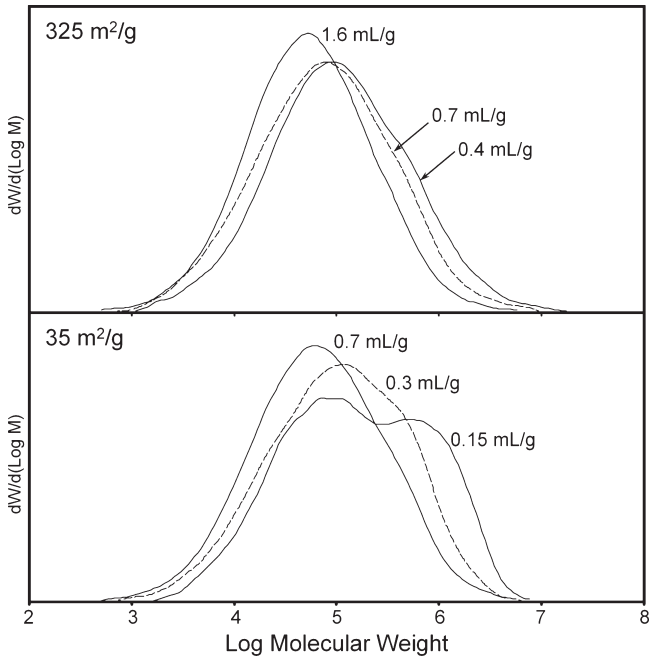

Figure 5. MW distribution of PE from two catalysts made by gelation of two types of colloidal silica particles, small and large, to produce high and low surface area. Samples of each gel were then dried in three different ways to also vary the pore volume.

matrix) from those of pore diameter (through which polymer must extrude during polymerization). Although Figure 4 shows pore volume to be the dominant variable in these tests, in the upper left graph, one can see that for a given PV, there is also a secondary tendency for the high-SA silicas to exhibit less surface activity than the low-SA silicas. Since the higher-SA materials have much wider pores for the same PV (because diam = 4PV/SA), we attribute this secondary relationship to the independent influence of pore diameter. Wider pores facilitate polymer egress in this series as a secondary influence. The molecular weight also seemed to exhibit this secondary influence, in which the high-SA samples (small pores) produced higher MW for a given PV. This secondary influence is less clear in the lower two frames in Figure 4.

It seems intuitive that the fragility of the silica matrix would depend on the number of connections each primary particle has with its neighbors (the CN), which is, in turn, determined by the pore volume. For a given CN, the pore volume is not related to the size of the primary particles, that is, the surface area, and so one might suppose that the strength is also unrelated to the surface area. It is interesting to consider this assumption in more detail.

In the upper part of Scheme 2, two hypothetical silicas are shown, each having cubic close packing, which provides a constant CN of 6 and pore volume of 0.52 mL/g (assuming a skeletal density of 2.3 g/mL for the primary silica particles.) In one case, however, the primary particle size is twice that in the other. This produces 8 times fewer primary particles in the same space, which lowers the surface area per gram by half. Because the primary particles are larger, so also are the holes between them so that the average pore diameter increases from 67 to 144 Å. We then attempted to evaluate the strength of each structure and compare it with the amount of force applied by polymer build-up in the pores during polymerization.

As polymerization begins, the forces on pore walls in the center of a typical 100-μm silica particle should be balanced. That is, the internal pressure trying to expand a pore is balanced by the opposite pressure from neighboring pores. However,

dx.doi.org/10.1021/cs2003033 |ACS Catal. 2011, 1, 1394–1407

Scheme 2. A Model Silica (upper drawing) in Which the Primary Particles Are in a Cubic Close Packing Matrix That Permits Calculation (lower graph) of the Relative Strength[a]

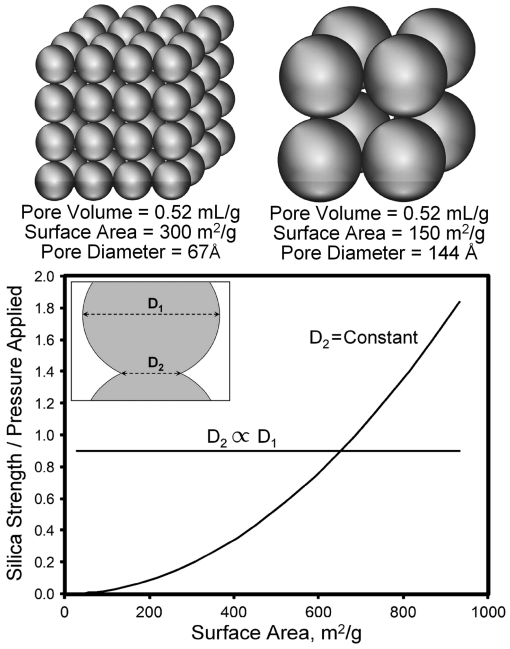

[a] Two cases are shown in the graph. In one case the contact area holding the spheres together is assumed to be independent of the primary particle size, and in the second case, it is assumed to be proportion to the particle size. In each case, the strength is plotted relative to the hypothetical pressure applied on a face by polymer build-up during polymerization.

forces exerted against pores in the exterior face of that 100-μm silica particle are not balanced, so we conclude that fragmentation would begin on the exterior plane of the matrix, and after those pores are ruptured, the process would continue toward the interior. Thus, to evaluate the fragility of the matrix, one must consider a two-dimensional plane of primary particles.

The strength of that plane should be the number of connections the outer plane has with its neighbors in the underlying plane of primary particles, multiplied by the strength of each connection. The force exerted by polymer accumulation that tries to break these connections is the pressure inside the pores multiplied by the two-dimensional area of the primary particles in the outer face (i.e., the area in the direction of the fracturing force). The lower part of Scheme 2 shows the predicted dependence on surface area (by variation of the primary particle size) of this measure of strength relative to the pressure exerted against it.

The strength of each particle-to-particle connection is assumed to be proportional to the area of fusion between the two particles, which is unknown. Two cases were considered. In the first case, all connections were considered to be equal, regardless of the size of the primary particles in contact. In the second case, the diameter of fusion (D_2) was considered to be proportional to the primary particle diameter (D_1). As shown in the lower part of Scheme 2, the first case predicts that the ability of the matrix to resist disintegration increases strongly with rising surface area, whereas in the second case, there is no dependence on surface area.

Exactly which case is more realistic is uncertain, but a similar problem can be considered which is in reverse, that is, the shrinkage of the matrix upon drying. Before the hydrogels in Figure 4 were dried, the pore water was either replaced by alcohol, or not, each of which produces a different degree of matrix shrinkage. Since the meniscus formed during drying pulls the primary particles together from the outside, this shrinkage can be considered as similar to the forces of disintegration during polymerization, except in reverse.

Table 2. Pore Volumes Obtained from Silicas Made with Various Sizes of Primary Particles[a]

		pore volume after drying from:	
reported particle diameter, nm	surface area, m^2/g	water, mL/g	*n*-propyl alcohol, mL/g
7	325	0.69	1.59
12	220	0.53	1.01
20	160	0.47	0.74
22	135	0.48	0.68
50	90	0.56	0.56
85	35	0.28	0.53

[a] Small particles seem to resist shrinkage better.

The final pore volumes obtained in this series of samples are listed in Table 2 as a function of primary particle size or surface area. Note that for a pore liquid, the smaller primary particles do seem to resist shrinkage better than those with large pores. This is in agreement with the direction shown in Scheme 2, case 1.

Keep in mind that these calculations assume that the internal pressure generated by polymer accumulation is not affected by the pore diameter. In reality, larger pores may actually facilitate polymer escape, thus diminishing the internal pressure.

Influence of Structural Coalescence. In the commercial manufacture of silica, another method of varying the surface area is more commonly used. Silica hydrogel is formed at relatively high SiO_2 content (20−30%) having high surface area (often ~1000 m^2/g or sometimes higher). After being washed free of residual sodium, the hydrogel is then treated at 60−90 °C in an aqueous solution in which the pH has been adjusted to 9−11 by the addition of NH_4OH, Na_2SiO_3, or NaOH. This treatment is sometimes called "alkaline aging" or "Oswald ripening". Depending on the severity of the treatment (pH, temperature, and time), one obtains varying degrees of coalescence of the silica structure.

Scheme 3 illustrates this process. Individual particles become fused together as silica is partially redissolved from the convex areas and redeposited into the concave areas, that is, the points of contact between primary particles. As a result of this process, the strength of the matrix is reinforced, the fine structure is lost, pore curvature changes from convex to concave, and the surface area declines. In this way, silica grades varying in surface area from 800 to 30 m^2/g are manufactured from a common hydrogel. Reinforcing the structure through Oswald ripening allows it to better withstand shrinkage during drying. Thus, alkaline aging makes it easier to maintain a high PV, and this was one of the original reasons for choosing such silicas for use as polymerization catalysts.

A similar coalescence or fusion of the structure can also be achieved through other means. For example thermal sintering of the dry silica at 900−1000 °C lowers the surface area in a similar way. Sintering can be considered as the early stages of melting the structure. Adding fluxing agents, such as sodium or fluoride, can accelerate the sintering process at lower temperatures, such as

dx.doi.org/10.1021/cs2003033 |ACS Catal. 2011, 1, 1394–1407

Scheme 3. Coalescence and Reinforcement of Silica Gel

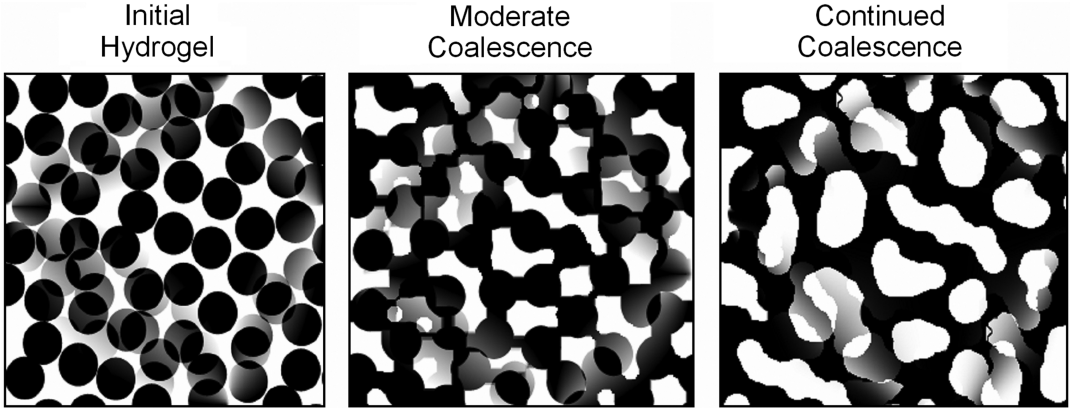

Table 3. Performance of Catalysts Made with W.R. Grace Reinforced Silicas (Sylox)[a]

surface area, m^2/g	pore vol, mL/g	av pore diam, Å	catalyst activity, g PE/g Cat/h	surface activity, g PE/m^2/h	mol wt (M_w), kg/mol	melt flow (HLMI), g/10 min	LCB (JC-α), LCB/10^6 C
257	1.43	222	1955	7.6	212	13.3	6.7
226	1.91	337	2552	11.3	233	12.9	8.6
147	1.67	454	2214	15.0	219	8.8	34.1
137	1.81	530	2392	17.5	230	3.5	46.0
105	1.59	606	1507	14.3	200	1.5	73.0
106	1.01	381	1463	13.8	230	1.6	82.3

[a] Note the extremely high levels of long chain branching.

400−600 °C.[50,51] Hydrothermal treatment, or "steaming" the silica at 500−900 °C, can also accomplish a similar coalescence of the structure. Sill another method of reinforcing the silica network is through a secondary deposition of silica onto an existing silica structure. This method is sometimes used with precipitated silicas (as opposed to gelled silicas).

Table 3 shows an example of the effect of lowering the surface area by reinforcement of the structure. These silicas were obtained from W.R. Grace under the Sylox name. The details of their preparation are proprietary, but these silicas are described as hybrids between gelled and precipitated silicas, in which secondary reinforcement is used. This method of preparation produces some unusually large pores. Moving down the table, the surface area decreases, indicating increased coalescence, the pore volume stays roughly constant, and the pore diameter increases.

In this series, the surface activity initially increases and then plateaus, suggesting that these large pores do facilitate egress of the polymer. Molecular weight remains approximately constant, but the amount of long-chain branching increases dramatically with reinforcement. In fact, this type of silica produced the highest degree of LCB we have observed from any Cr/silica catalyst. Because of the high LCB, the melt flow declined even though the molecular weight was constant. Long-chain branches tend to become entangled with other chains, thus retarding the flow of the molten polymer. Therefore, in this series, lowering the surface area produced some major changes in the polymer, which is unlike the result in Figure 4.

In another study, shown in Figure 6, commercial silicas in which the surface area was lowered by alkaline aging a common hydrogel from ~800 to 30 m^2/g were obtained from W.R. Grace. Two similar samples, made by aqueous gelation and having a surface area of 1100 and 1700 m^2/g, were also included in the study. Pore volume was maintained relatively constant at 1.0 or 1.6 mL/g, as indicated. Thus, as the silica samples became more reinforced, surface area was lost, and the pore diameter consequently increased.

The results of this study are plotted in Figure 6 against pore diameter, which produced an excellent fit. They could also have been plotted against the surface area, but this resulted in separate lines for each pore volume, suggesting that pore diameter may be the more relevant variable in this series. In the upper left, surface activity first increases with higher pore diameter, then plateaus, then it eventually declines at the most extreme level of reinforcement. It seems likely in this series that this initial rise in activity can be attributed to enhanced egress of polymer and not to enhanced fragility, because (unlike the series in Figures 2 and 4) the strength of the network in this series should rise with pore diameter due to progressively higher levels of reinforcement.

The middle plateau in activity suggests that all of the surface does participate in the reaction, even though the matrix strength is increasing. This further suggests that the large pores allow adequate egress of polymer from catalyst fragments. The loss in activity at the most extreme level of reinforcement might be interpreted as due to poor fragmentation.

The polymer properties are also plotted in Figure 6 and seem to be highly dependent on the degree of reinforcement. Molecular weight initially declines, which coincides with the rise in activity. Then it plateaus and eventually rises a little, again behaving similar to the activity. In contrast, the degree of long-chain branching rises steadily with increased coalescence. In fact,

dx.doi.org/10.1021/cs2003033 |ACS Catal. 2011, 1, 1394–1407

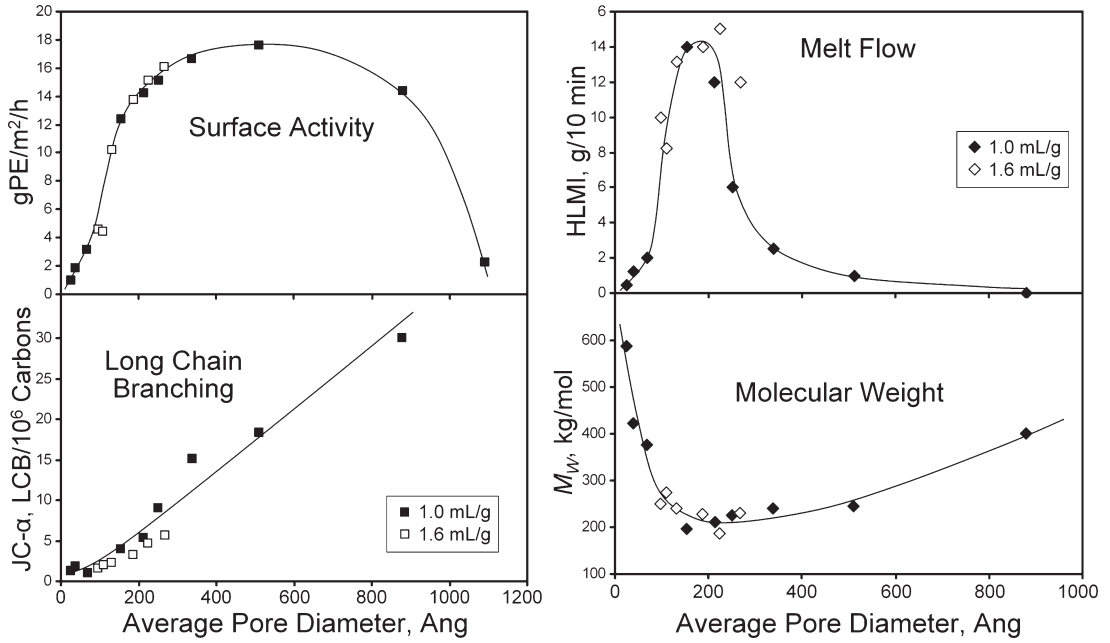

Figure 6. Performance of catalysts made by alkaline aging a common silica hydrogel to achieve coalescence, pore expansion, and loss of surface area.

one can almost see two lines representing the two pore volumes. As shown in Table 3, LCB seems to be quite sensitive to the degree of reinforcement. The melt flow goes through a sharp peak at a pore diameter of ~200 Å. This is the result of (1) the initial decline in molecular weight, which increases the fluidity, and then (2) the later rise in LCB, which entangles and retards flow in the molten polymer.

Many other methods of coalescence have also been tested in this laboratory with similar results. For example some silicas were thermally sintered at 850−950 °C for varying times to lower the surface area and increase the pore diameter. Then they were soaked in liquid water to rehydrate the surface, followed by impregnation of Cr, drying, and then the normal activation by calcination. In other tests, silicas were steam-treated at 600−900 °C, followed by rewetting and Cr impregnation. Still other tests involved fluxing at 700−850 °C with high levels of sodium, followed by washing to remove the Na and rehydrate the silica. Cr was then impregnated, and the catalyst was activated in the normal way. These various methods of reinforcement all produced high levels of LCB, which could have been plotted in Figure 6 to produce a similar line. Activity, molecular weight, and melt flow also behaved like that in Figure 6.

Figure 7 shows the change in MW distribution observed from the polymers in Figure 6. GPC curves from the sample having pore diameter of 180 Å up to 880 Å are shown. The increased molecular weight observed from coalescence of the catalyst was again not because of a shift of the entire curve but, instead, from the development of a high-MW shoulder. In fact, a bimodal MW distribution was obtained from the most severely reinforced catalyst.

On the other (left) side of the 200 Å optimum in Figure 6, the same changes in the MW distribution were observed at smaller pore diameter. That is, a high-MW shoulder was initially present from the least reinforced samples (those having smallest pore diameter and highest surface area), but it declined with rising diameter and eventually disappeared at 200 Å diameter. This behavior again suggests that two types of polymer are produced

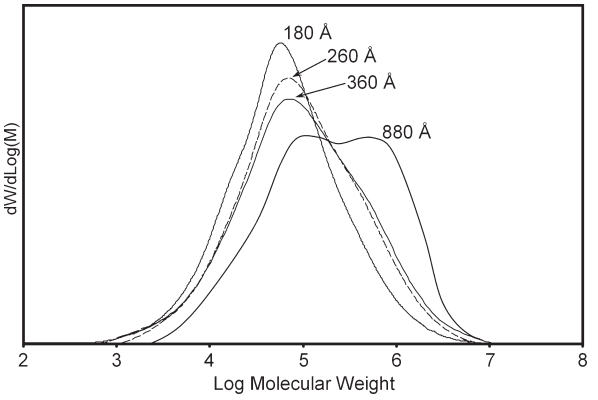

Figure 7. MW distributions of PE from silicas that were alkaline-aged to varying degrees to coalesce and strengthen the catalyst matrix.

whose relative contributions depend somehow on the porosity or structure of the catalyst.

In another experiment, samples of chromia−silica−titania hydrogel were alkaline-aged at pH 10 and 85 °C for increasing amounts of time to enhance coalescence of the structure and consequently lower the surface area. After each sample had been alkaline aged for its particular time, it was then split into other samples that were each dried in a different way, designed to produce varying levels of pore shrinkage. In this way, both surface area and pore volume were varied independently. Afterward, each sample was calcined at 800 °C and tested for polymerization activity. Table 4 lists the results.

For a given method of drying, one can see that the pore volume rises with increased coalescence, indicating greater strength to withstand shrinkage. Thus, the PV is enhanced by lowering the surface area. The melt index of the polymers made by these catalysts is also listed in Table 4. It is interesting that, when plotted against the pore diameter, the melt index produces a single line with an excellent fit, regardless of the alkaline aging

dx.doi.org/10.1021/cs2003033 |ACS Catal. 2011, 1, 1394–1407

Table 4. Dependence of Polymer Melt Index on Catalyst Average Pore Diameter[a]

alkaline treatment time, h	pore liquid	surface area, m^2/g	pore volume, mL/g	pore diameter, Å	melt index, g/10 min
0	water	503	0.69	55	0.00
0	surfactant	510	0.88	69	0.26
0	*n*-propyl alcohol	531	1.78	142	1.20
0	1-hexanol	499	2.01	161	1.64
1	water	491	0.69	56	0.00
1	*n*-propyl alcohol	523	1.75	134	1.40
3	water	452	0.71	63	0.15
3	*n*-propyl alcohol	461	1.81	157	1.50
11	water	410	0.81	79	0.35
11	surfactant	395	1.07	108	0.66
11	*n*-propyl alcohol	390	1.81	186	1.80
27	water	367	0.86	93	0.60
27	surfactant	375	1.26	134	1.06
27	*n*-propyl alcohol	364	1.92	211	2.00
27	1-hexanol	357	2.17	243	2.10

[a] Cr/silica−titania hydrogel samples were alkaline-aged to coalesce and reinforce the structure, then the pore water was replaced by other liquids before the gel was dried.

Table 5. Activity and Polymer Properties from Two Silicas, Showing the Independent and Additive Influence of Both Porosity and Calcination Temperature

calcination temp, °C	activity, kg/g/h	surface activity, g/m2/h	molecular weight, M_w kg/mol	melt flow (HLMI), g/10 min	LCB/10^6 C
Silica A: 622 m^2/g, 1.05 mL/g, 70 Å Pore Diameter, No Coalescence					
500	1200	1.9	770	0.1	0.5
600	2300	3.7	530	0.3	1.5
700	2700	4.3	380	1.6	3.5
800	3100	5.0	300	4.6	6.5
900	2800	4.5	220	10.2	12.0
Silica B: 288 m^2/g, 1.63 mL/g, 226 Pore Diameter, Strong Coalescence					
500	1100	3.8	365	1.5	1.5
600	1500	5.2	270	4.3	5.0
700	2000	6.9	225	8.5	10.0
800	2600	9.0	190	16.6	18.0
900	2000	6.9	165	21.1	25.0

time. The shape of this line is identical to that of the melt flow in Figure 2. When the melt index data in Table 4 is plotted against pore volume instead of pore diameter, a band of points is observed that rises with rising PV, as one would expect. However, the fit is relatively poor, even though the overall trend is visible. This indicates that in this series of catalysts, pore diameter successfully captures the MI dependence on both PV and fragment pore diameter, whereas PV alone is not completely adequate.

Other Variables. Other catalyst variables are known to influence activity,[1] polymer molecular weight and MW distribution,[1,3] and the amount of long-chain branching in the polymer[43] as well as the pattern and amount of comonomer incorporation.[52] For example, the addition of titania to Cr/silica increases catalyst activity, lowers the molecular weight, broadens the MW distribution (on the low-MW side), and usually increases elasticity (LCB). Likewise, raising the calcination temperature tends to improve activity, lowers the molecular weight, narrows the MW distribution, and increases LCB. Both activation temperature and titania are thought to modify the active site population and character. These responses occur independently of, and in addition to, the influence of catalyst porosity that has been reported here.

Thus, the same influence of catalyst porosity is observed on activity and polymer properties regardless of the activation temperature or the presence of titania. Both have been varied some in this report as an example. Many other variables also influence the catalyst independently of the role of porosity, such as the Cr concentration, treatment with poisons or cocatalysts, or copolymerization. The influence of porosity described in this paper can be considered as additive to these other responses, indicating that it occurs though a different mode of action.

Table 5 shows an example of this. Catalysts were made from two silicas, differing in porosity in which one was highly coalesced, whereas the other was not alkali-treated. This treatment produced a higher pore volume, lower surface area, and wider average pore diameter in the former catalyst. After impregnation of 1 wt % chromium, both catalysts were then calcined at temperatures from 500 to 900 °C. Each was then tested for polymerization activity, and the results are shown in

dx.doi.org/10.1021/cs2003033 |ACS Catal. 2011, 1, 1394–1407

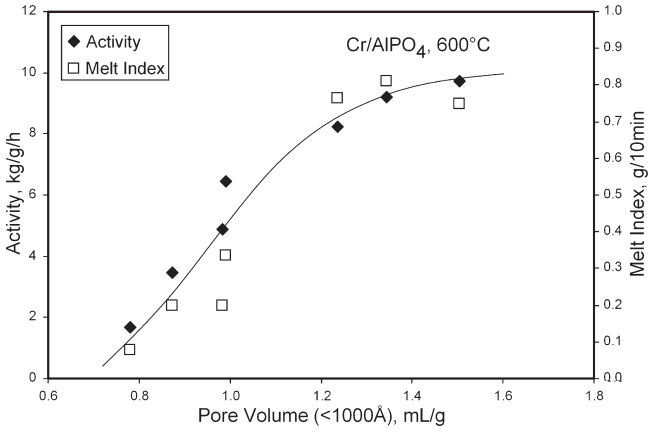

Figure 8. Activity and melt index of polymer from Cr/aluminophosphate catalysts that were made by the cogelation of Al^{3+}, PO_4^{3-}, and Cr^{3+} ions. The water in this gel was exchanged with various organic solvents that differed in surface tension to vary the pore volume upon drying. Catalysts were activated at 600 °C.

Table 5. Notice that the surface activity increases with temperature for both silica grades. Likewise, the molecular weight decreases, the MW breadth narrows, and the amount of LCB in the polymer increases. Notice also that the porosity has the expected influence, regardless of calcination temperature. The higher PV and wider pores produce higher surface activity and lower molecular weight at each temperature. The more reinforced structure produces higher levels of LCB at each temperature. Thus, the porosity and the calcination temperature each have their own independent influence, and the two effects are additive.

Other Supports. The trends described above were developed using Cr/silica catalysts. The initial primary particles are thought to be amorphous spheres that link into a network during gelation and later coalesce into a stronger framework during alkaline aging or other processing.[49] Other supports, such as alumina or the aluminophosphates, may not start with the same particles or undergo the same processes during catalyst formation. Thus, it is interesting to examine other supports to observe similarities and differences.

Over the years, we have accumulated much experimental data that indicates that most of these trends based on silica also apply to the aluminophosphates. Since aluminum phosphate is isoelectronic and isostructural with silica, it is perhaps expected that stoichiometric $AlPO_4$ would behave similarly to silica as a polymerization catalyst. However, these trends are also seen from nonstoichiometric aluminophosphates, in which the P/Al molar ratio is 0.6, 0.4, or even 0.2.

Figure 8 shows the results of experiments in which a Cr/aluminophosphate hydrogel (P/Al = 0.6) was dried by first replacing the pore water with alcohol−water mixtures of varying water content to vary the surface tension during drying and, thus, the final PV. The dried catalysts were then calcined at 600 °C and then tested for polymerization activity with 8 ppm of triethylboron cocatalyst. The plot in Figure 8 shows that activity and the melt index rise with increasing pore volume (or pore diameter), eventually leveling off just as was seen in Figure 2 from Cr/silica.

Actually, the pore volume plotted in Figure 8 was not obtained by N_2 sorption, but instead, by mercury penetration. This is the volume found in pores smaller than 1000 Å. Molecular weight and activity from this experiment and many others were plotted against the volume inside other pore sizes. For example <10 000 Å also provided an excellent fit, but <100 000 Å did not do as well. No correlation was noted from the <100 Å range in this series. These data suggest that it is the mesopores that influence the catalyst activity (and polymer properties) most.

Table 6. Activity and Polymer Properties from Metallocene Activated by Acidic Aluminas of Varying Pore Volume

pore vol, mL/g	surface area, m^2/g	pore diam, Å	activity, kg/g/h	surface activity, $g/m^2/h$	HLMI, g/10 min
1.38	304	182	7300	24.0	2.4
1.21	286	169	5144	18.0	2.1
1.11	309	144	3500	11.3	0.8
0.80	293	109	2892	9.9	0.6
0.45	285	63	800	2.8	0

Aluminas were also investigated as polymerization catalyst supports. Here, too, the activity is governed by the pore volume. The chemistry of Cr/alumina catalysts tend to produce ultra-high-MW polymers, making the molecular weight and the flow behavior very difficult to measure. Nevertheless, the PV does seem to control molecular weight in a way similar to the silicas.

When compared with Cr/silica of the same surface area and pore volume, Cr/alumina catalysts usually produce very low amounts of long-chain branching. LCB levels are lowered by 1−2 orders of magnitude. This might be attributed to a different active site population on alumina, but this behavior is also sometimes seen from metallocene catalysts, as well (see below). Thus, another possible explanation is the difference in structure between alumina and silica. The alumina nanostructure is often a loose agglomeration of small platelets, rather than the fusion of silica spheres into a strong mass. If true, this connection of LCB with a weak alumina structure would agree with (and be an extrapolation of) the established trends observed on silica.

Similarly, various clays were also tested as supports for chromium catalysts.[53] The bentonites are interesting because the structure consists not of fused particles, but of thin sheets that are not chemically connected and are thus are easily separated. When used as a support for chromium catalyst, bentonite produced an active catalyst. At low activation temperature (300 °C) Cr/bentonite produced extremely low levels of LCB, which might be attributed to the unusual structure. After the temperature was raised, however, to the point where clay pots are "fired" to fuse the structure, these Cr/bentonite catalysts produced extremely high LCB levels. One can appreciate the large magnitude of the change in the following progression: 300 °C produced only 0.1 LCB/10^6 carbons; 500 °C produced 1.0 LCB/10^6 carbons; 600 °C produced 4 LCB/10^6 carbons, and finally, 700 °C produced 20 LCB/10^6 carbons. Thus, the bentonite results seem to confirm the trend observed (and extrapolated) from the silicas.

Other Catalysts. It is perhaps not surprising, then, that supported metallocene catalysts often display some of these same responses to catalyst porosity, especially the activity and the amount of long-chain branching. This is another confirmation that the physical effects of porosity on polymerization are independent and additive to the chemical influence of these other variables.

Table 6 shows an example of the effect of catalyst porosity on the activity of a metallocene catalyst. Five aluminas, varying in pore volume, were treated with ammonium sulfate and then

dx.doi.org/10.1021/cs2003033 |ACS Catal. 2011, 1, 1394–1407

Scheme 4. Strained Agostic β-H Coordination Position Necessary As a Precursor for Chain Termination

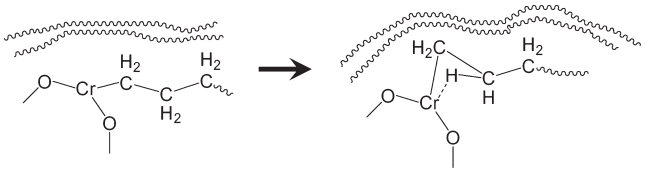

calcined. This provides sufficient surface acidity to activate metallocenes.[54] In this example, 2-(η-5-cyclopentadienyl)-2(η-5-fluorenyl)hex-5-ene zirconium dichloride was used as the metallocene to make 1-hexene copolymer having a density of 0.918 g/mL. This metallocene was chosen because these polymers contain low levels of LCB.[55] One can see that the activity increases significantly with rising pore volume, which is a repetition of the trends noted earlier from Cr/silica (Figures 2 and 4, Tables 1 and 4) and from Cr/aluminophosphate (Figure 8).

The melt index (HLMI) obtained from these catalysts is also shown in Table 6. Again, the melt index increased with catalyst pore volume, as it does for Cr/silica (Figures 2 and 4, Table 1) and for Cr/aluminophosphate (Figure 8). However, the tendency of metallocenes to generate hydrogen during polymerization,[56] which then can terminate chains, makes the interpretation of the MW trend less certain.

Long-chain branching by metallocenes also seems to follow some of the dependence of porosity, as was observed with Cr/silica catalysts. For example, LCB is higher when the metallocene is activated by an acidified silica than it is when activated by acidified alumina or by a clay. This is in agreement with trends observed from chromium catalysts. Thus, the effect of porosity on metallocene catalysts is an area that will be the subject of future investigations.

CONCLUSIONS

In this paper, we have presented new data and also summarized data from two earlier studies in an attempt to consider all the major physical characteristics of Cr/silica that determine its polymerization behavior. The structure of the silica has been shown to play an important role not only to the activity of Cr/silica catalysts, but also (and less intuitively) to all the major features of the polymer behavior. Most of these important commercial polymer characteristics can be considered as derivatives of three underlying molecular features: (1) its molecular weight, (2) its MW distribution, and (3) the amount of long-chain branching it contains. When all of this present and earlier data are considered together, one can see several underlying connections that tie the different variables together into a unified picture. Some generalizations can be made and are described below, about the response of these four primary polymerization variables to catalyst porosity.

Surface Participation. The strong influence of porosity must derive from two possible causes: (1) It affects the fragility of the catalyst, which in turn may control the size of the fragments produced by disintegration during polymerization; and (2) the pore width inside the resulting fragment must influence the ease by which polymer produced within the interior of the fragment is "extruded" out of the pores (perhaps even in a semimolten or excited mobile state). Both phenomena probably combine to determine what fraction of the internal surface is allowed to contribute to the polymerization.

By studying the catalyst activity expressed per unit of BET surface area, one can gauge how much of the surface contributes to the polymerization reaction. When the most active (i.e., "polymerization-grade") silica gels are compared with pyrogenic nanoscale silicas, it is clear that the polymerization-grade silicas fragment until all of the surface is available. But even these silicas still display a dependence of polymer character on the pore diameter. Thus, the interior of the fragments must also contribute.

A large pore diameter (>200−300 Å) seems to be necessary for maximum surface participation, which suggests that egress of polymer chains from within the fragments is important. In the pore range of 200−1000 Å, a near-flat, maximum activity is obtained (Figures 2, 6, and 8, Tables 1 and 3). When the pore diameter is <200 Å, however, even inherently weak silicas (i.e., having high PV) do not display full surface participation (Figures 2, 4, and 6, and Table 1, <200 Å). This indicates the importance of the pore diameter in these fragments.

On the other end of the scale, highly reinforced catalysts having a low PV are also less active, despite the very wide pore diameter (Figure 6, >800 Å). This suggests that these silicas could not rupture to a sufficient degree to permit total polymer egress from the resulting fragments.

Molecular Weight. Polymer molecular weight followed a similar trend. Pores smaller than ∼200 Å tended to make long PE chains (Table 1, Figures 2 and 6). This occurred even at high PV using inherently weak silicas. In many experiments (some not shown here), the molecular weight decreased with rising pore diameter up to about 200 Å, after which point MW became relatively constant.

Thus, polymer chains become longer when they are produced under the more restricted and crowded conditions. A possible explanation that we propose to explain this behavior is that in such crowded pores, polymer chains are inhibited from assuming the agostic β-H coordination that is a precursor for chain termination. This is illustrated in Scheme 4. Hence, chains would tend to grow longer under such crowded conditions, even with reduced monomer access.

On the other end of the scale, highly reinforced silicas (wide pores but probably large fragments) also yielded high molecular weight polymer (Figures 6, >800 Å). Again, we propose that this is due to the crowded conditions inside pores where the polymer is formed. The larger pores facilitate polymer egress, but under extreme reinforcement, fragments become large enough that egress again becomes difficult despite the wide pores.

A possible exception to this view is the data in Figure 4, where molecular weight seemed to correlate better with pore volume than with pore diameter. These catalysts were made from colloidal silica particles that were gelled and not coalesced or otherwise reinforced. Thus, in this series, the strength of the silica (and perhaps the extent to which it fragments) is especially closely connected to the PV. Even there, however, one can see the influence of pore diameter (independent of pore volume) if one looks carefully at Figure 4.

MW Distribution. In all of these diverse experiments, the higher average MW was caused not by a shift in the MW distribution but, instead, by the development of a high-MW shoulder (Figures 3, 5 and 7). This fact suggests that two types of polymer are formed, and the relative amount of each is determined by the catalyst porosity. We propose that the high-MW

dx.doi.org/10.1021/cs2003033 |ACS Catal. 2011, 1, 1394–1407

shoulder is probably made *inside* the fragments and extruded from he pores, whereas the normal polymer is made on the *exterior* of the fragments. Thus, the more highly active catalysts would tend to disintegrate until the fragments are small enough to expose nearly all the surface so that they produce normal polymer. However, as the pores become smaller or the catalysts become stronger, they may not fracture to the same extent so that larger fragments are produced, forcing the polymer to extrude from pores as it is formed.

It is the smaller (<200 Å) pores that are most crowded and that therefore have the strongest tendency to produce higher MW. This explains why the high-MW shoulder correlates nicely with surface participation.

Long-Chain Branching. The production of long-chain branching also must be due to polymer growth inside pores. When a chain is terminated inside a pore, the vinyl end group can collide with pore walls until it is finally "extruded" out of the pore. During this time, there is a chance of contacting another site inside the same pore, which then incorporates into another growing chain as a long-chain branch.

It is useful to consider the dimensions involved in polymer growth. Although a typical pore diameter might be 100−200 Å, the average polymer chain is orders of magnitude longer, such as 600 000 Å (M_w), or >2×10^6 Å for a significant fraction of the polymer. A pore cannot contain even one polymer molecule (even when it is in a folded or crystalline state). Instead, the growing chain must extrude out of the pores as it is formed. Thus, it seems likely that only a few growing polymer chains could simultaneously extrude from a pore. During their escape, vinyl end groups have a chance of contacting other sites on the pore wall, where they may be incorporated. In fact, a polymer chain generated inside a pore cannot fold on itself in the usual way, and its temporary unnatural state may contribute to LCB formation.

Now let us consider the number of active sites that could be inside a pore. The average distance between active sites is ∼5 nm (assuming 300 m^2/g, 1% Cr, and 10% of the Cr is active). This corresponds to ∼1 active site per pore cavity for the geometry shown in Scheme 2. Thus, the average number of active sites per pore could vary from less than one to several, depending on the porosity. This is also consistent with the increase in LCB observed when the Cr loading is raised,[43] which would increase the number of active sites per pore cavity.

Using again the model geometry in Scheme 2, we see that silicas having a high surface area (but equal PV) have fewer active sites per pore cavity. This is consistent with the rise in LCB seen with dropping surface area in Figures 4 and 6 and Table 3. In fact, we see that an increasing pore diameter, which is usually (but not always) accompanied by a dropping surface area, also increases the number of sites per pore cavity, which is consistent with Figure 6 and Table 3.

In addition, a highly reinforced silica matrix, as in Table 3 or Figure 6, may inhibit disintegration, causing larger fragments and increasing the effective length of the pore. This, too, would enhance the probability of a chain end's being incorporated as LCB. Indeed, LCB seems to be most influenced by the degree of silica reinforcement. This may be due to the fact that on these catalysts, proportionally more of the polymer is made inside the pores.

However, low pore volume, as in Table 1 and Figures 2 and 4, also tends to increase LCB if other variables are equal. This, too, is seen as the result of increased strength inhibiting particle disintegration, producing larger fragments, so that more of the polymer is made inside pores, which being longer contain more active sites. This is consistent with the observed loss of surface participation, as in Table 1 and Figures 2 and 4.

Independence of LCB and MW. Thus, the origin of LCB and of high MW are related, and the two follow some of the same trends. But it is also important to realize that their origins are not exactly the same, and consequently, there are also some differences. For example, LCB does not always correlate with the high-MW shoulder (Table 3 and Figure 6). Small pores can produce very high MW but still very low LCB. On the other hand, increasing the pore diameter beyond 200 Å continues to increase LCB while doing nothing to the MW. Thus, as described above, the two mechanisms are related, but not identical. MW is increased when the pores become "crowded" enough to inhibit surface activity. LCB, on the other hand, is increased when the pore cavity contains more active sites (i.e., becomes larger) and also when the matrix is reinforced enough to inhibit fragmentation.

Resisting Surface Tension. In this paper, we have proposed the idea that forces resisting pore rupture during polymerization are inversely parallel to those resisting pore shrinkage by surface tension during drying. Consequently, we find a good inverse correlation between pore shrinkage and polymerization activity. This relationship is especially helpful in understanding the role of pore diameter, independent of pore volume. It explains why silicas of equal pore volume but different pore diameter can perform differently. Their strengths are, indeed, different.

Other Theories Considered. *1. Diffusion.* Other, perhaps more intuitive, explanations have also been considered, but without success. For example, it is reasonable to ask if the observed change in polymer properties could derive from limited monomer access to the active sites as catalyst porosity is varied. Actually, lowering the external ethylene concentration, to mimic the lower monomer concentration expected in small pores, does tend to raise LCB as is observed from low PV catalysts. But it also tends to lower MW, which is contrary to Figures 2, 4, 6, and 8 and Tables 1, 4, 5, and 6.

From this idea of diffusion controlling polymer properties, one would also expect polymer properties to correlate with surface activity. MW does seem to correlate, but LCB does not. For example, in Figure 6 activity first rises as LCB rises, then activity plateaus as LCB rises, and finally activity drops as LCB rises. Likewise in Figure 6 and Table 3, many catalysts exhibited high LCB even with full surface participation. Thus, ethylene diffusion does not predict the observed LCB or MW responses.

2. Localized Overheating. Alternatively, localized overheating within a particle due to high activity would tend to lower the molecular weight. That is, MW should correlate with surface activity. But it does not. The MW changes of the magnitude seen here would require very large rises in temperature of, say, 20−30 °C, which is not predicted by the models.[57] Furthermore, by this reasoning, one might expect catalysts of different particle size to exhibit even more variability due to heat build-up. But in studies with 200 μm catalyst particles down to 2−5 μm particles, we have seen comparatively little change in MW. Furthermore, this explanation predicts no influence on LCB.

Universal Principles. Finally, it is important to recognize that these principles apply to other supports when impregnated with chromium and to other catalysts, such as metallocenes. It is clear that these physical phenomena, although independent, are also superimposed onto the chemistry of the catalyst. Thus, variations in the Cr-catalyst recipe (bonding and ligand field from the

support, calcination history, and reactor additives), or in the metallocene choice (steric and electronic influences by the ligand), can influence MW and LCB. But this chemical contribution is combined with that of the physical structure of the support, which can have more or less significance in comparison.

AUTHOR INFORMATION

Corresponding Author

*E-mail: Max.McDaniel@sbcglobal.net.

REFERENCES

(1) McDaniel, M. P. *Adv. Catal.* **2010**, *53*, 123–606.

(2) Hogan, J. P.; Kitchen, A. G. U.S. Patent 3,225,023; December 21, 1965 to Phillips Petroleum Co.

(3) Hogan, J. P.; Norwood, D. D.; Ayres, C. A. *J. Appl. Polym. Sci.: Appl. Polym. Symp.* **1981**, *36*, 49–60.

(4) Niegisch, W. D.; Crisafulli, S. T.; Nagel, T. S.; Wagner, B. E. *Macromolecules* **1992**, *25*, 3910.

(5) Whitacker, H. L.; Wills, G. B. *J. Appl. Polym. Sci.* **1969**, *13*, 1921.

(6) McDaniel, M. P. *J. Polym. Sci.: Polym. Chem. Ed.* **1981**, *19*, 1967.

(7) Floyd, S.; Heiskanen, T.; Taylor, T. W.; Mann, G. E.; Ray, W. H. *J. Appl. Polym. Sci.* **1987**, *33*, 1021.

(8) Aguado, J.; Calleja, G.; Carrero, A.; Moreno, J. *Appl. Catal., A* **2007**, *316*, 22–31.

(9) Aguado, J.; Calleja, G.; Carrero, A.; Moreno, J. *Microporous Mesoporous Mater.* **2010**, *131*, 294–302.

(10) Aguado, J.; Calleja, G.; Carrero, A.; Moreno, J. *Chem. Eng. J.* **2008**, *137*, 443–452.

(11) Debling, J. K.; Ray, W. H. *Ind. Eng. Chem. Res.* **1995**, *34*, 3466.

(12) Hutchinson, R. A.; Chen, C. M.; Ray, W. H. *J. Appl. Polym. Sci.* **1992**, *44*, 1389.

(13) Hutchinson, R. A.; Chen, C. M.; Ray, W. H. *J. Appl. Polym. Sci.* **1992**, *44*, 1389.

(14) Wagner, B. E.; Niegisch, W. D. *Polym. Mater. Sci. Eng.* **1991**, *64*, 139.

(15) Ruddick, V. J.; Badyal, J. P. S. *J. Phys. Chem. B* **1997**, *101*, 1791.

(16) Dalla Lana, I. G.; Szymura, J. A.; Zielinski, P. A. *Stud. Surf. Sci. Catal.* **1993**, *75* (New Frontiers in Catalysis, Pt. C), 2329–2332.

(17) Szymura, J. A.; Zielinski, P. A.; Dalla Lana, I. G. *Catal. Lett.* **1992**, *15*, 145.

(18) Szymura, J. A.; Zielinski, P. A.; Dalla Lana, I. G. *Stud. Surf. Sci. Catal.* **1992**, *73* (Prog. Catal.), 69.

(19) Szymura, J. A.; Dalla Lana, I. G.; Fiedorow, R.; Zielinski, P. A. *Macromolecules* **1996**, *29*, 3103–3110.

(20) Follestad, A.; Helleborg, S.; Almquist, V. *Stud. Surf. Sci. Catal.* **1990**, *56* (Catal. Olefin Polym.), 63–85.

(21) Davidson, T. *Polym. Lett.* **1970**, *8*, 855.

(22) Conner, W. C.; Ferrero, M.; Webb, S.; Sommer, R.; Chiovetta, M.; Jones, K.; Spanne, P. *Stud. Surf. Sci. Catal.* **1993**, *75* (New Frontiers in Catalysis, Pt. B), 1827–1830.

(23) Jones, K. W.; Spanne, P.; Lindquist, W. B.; Conner, W. C.; Ferrero, M. *Nucl. Instrum. Methods Phys. Res., Sect. B* **1992**, *B68*, 105.

(24) Webb, S. W.; Weist, E. L.; Chiovetta, M. G.; Laurence, R. L.; Conner, W. C. *Can. J. Chem. Eng.* **1991**, *69*, 665.

(25) Conner, W. C.; Webb, S. W.; Spanne, P.; Jones, K. W. *Macromolecules* **1990**, *23*, 4742.

(26) Conner, W. C.; Weist, E. L.; Ali, A. H.; Chiovetta, M.; Laurence, R. L. Transition Metal Catalyzed Polymerization. *Proceedings of the 2nd International Symposium*, Akron, OH, 1986; Quirk, R. P., Ed.; Cambridge University Press: Cambridge, UK, 1988; pp 417−427.

(27) Webb, S. W.; Conner, W. C.; Laurence, R. L. *Macromolecules* **1989**, *22*, 2885.

(28) Weist, E. L.; Ali, A. H.; Conner, W. C. *Macromolecules* **1987**, *20*, 689.

(29) Jones, K. W.; Spanne, P.; Webb, S. W.; Conner, W. C.; Beyerlein, R. A.; Reagan, W. J.; Dautzenberg, F. M. *Nucl. Instrum. Methods Phys. Res., Sect. B* **1991**, *B56-B57* (Pt. 1), 427.

(30) Witt, D. R. U.S. Patent 3,900,457; Aug. 19, 1975.

(31) Short, J. N.; Witt, D. R. U.S. Patent 4,081,407, Mar. 28, 1978; U.S. Patent 4,152,503, May 1, 1979, both assigned to Phillips Petroleum Co.

(32) Schmidt, H.; Riederer, W.; Krauss, H. L. *J. Prakt. Chem./Chem.-Ztg.* **1996**, *338*, 627.

(33) Ballard, D. G. H. *J. Polym. Sci., Polym. Chem. Ed.* **1975**, *13*, 2191.

(34) Ballard, D. G. H.; Jones, E.; Wyatt, R. J.; Murray, R. T.; Robinson, P. A. *Polymer* **1974**, *15*, 169.

(35) Calleja, G.; Aguado, J.; Carrero, A.; Moreno, J. *Catal. Commun.* **2005**, *6*, 153.

(36) Webb, S., Conner, W. C., Lawerence, R. L., *Proceedings of the Third Berlin International Workshop on Polymer Reaction Engineering*, 1989, pp 381−399.

(37) Thüne, P. C.; Niemantsverdriet, J. W. *Isr. J. Chem.* **1998**, *38*, 385.

(38) Thüne, P. C.; Loos, J.; Lemstra, P. J.; Niemantsverdriet, J. W. *J. Catal.* **1999**, *183*, 1.

(39) Loos, J.; Thüne, P. C.; Niemantsverdriet, J. W.; Lemstra, P. J. *Macromolecules* **1999**, *32*, 8910.

(40) Thüne, P. C.; Loos, J.; Weingarten, U.; Muller, F.; Kretschmer, W.; Kaminsky, W.; Lemstra, P. J.; Niemantsverdriet, J. W. *Macromolecules* **2003**, *36*, 1440.

(41) Ferrero, M. A.; Webb, S. W.; Conner, W. C.; Bonardet, J. L.; Fraissard, J. *Langmuir* **1992**, *8*, 2269.

(42) Estenoz, D. A.; Chiovetta, M. *Polym. Eng. Sci.* **1996**, *36* (17), 2206.

(43) McDaniel, M. P.; Rohlfing, D. C.; Benham, E. A. *Polym. React. Eng.* **2003**, *11* (2), 105–135.

(44) McDaniel, M. P.; Collins, K. S. *J. Catal.* **2009**, *261*, 34–49.

(45) McDaniel, M. P.; Collins, K. S. *J. Polym. Sci., Part 1: Chem.* **2009**, *47* (3), 845–865.

(46) Yu, Y.; Rohlfing, D. C.; Hawley, G. R.; DesLauriers, P. J. *Poly. Prepr.* **2003**, *44*, 50.

(47) Bird, R. B.; Armstrong, R. C.; Hassager, O. *Dynamics of Polymeric Liquids*; Fluid Mechanics; John Wiley & Sons: New York, 1987; Vol. 1.

(48) Janzen, J.; Colby, R. H. *J. Mol. Struct.* **1999**, *485/486*, 569.

(49) Iler, R. K. *The Chemistry of Silica: Solubility, Polymerization, Colloid and Surface Properties, and Biochemistry*; Wiley: New York, 1979.

(50) McDaniel, M. P.; Witt, D. R.; Benham, E. A. *J. Catal.* **1998**, *176*, 344–351.

(51) Witt; D. R.; Benham; E. A.; McDaniel, M. P. U.S, Patent 5,284,811, February 8, 1994; U.S.Patent 5,444,132, August 22, 1995; both to Phillips Petroleum Co.

(52) Delauriers, P. J.; McDaniel, M. P. *J. Polym. Sci.* **2007**, *45*, 3135–3149.

(53) Shveima, J. S., U.S. Patent 5,376,611, December 27, 1994; U.S. Patent 5,502,265, March 26, 1996; U.S. Patent 6,403,516, June 11, 2002; U.S. Patent 6,617,404, September 9, 2003; all assigned to Phillips Petroleum Co.

(54) McDaniel, M. P.; Jensen, M. D.; Jayaratne, K.; Collins, K. S.; Benham, E. A.; McDaniel, N. D.; Das, P. K.; Martin, J. L.; Yang, Q.; Thorn, M. G.; Masino, A. P. Metallocene Activation by Solid Acids. In *Tailor-Made Polymers: Via Immobilization of Alpha-Olefin Polymerization Catalysts*; Severn, J., Chadwick, J.C., Eds.; Wiley-VCH: Weinheim, 2008; Vol. XVI; Chapter 7; pp 171−210; ISBN: 978-3-527-31782-0.

(55) Yang, Q.; Jensen, M. D.; McDaniel, M. P. *Macromolecules* **2010**, *43*, 8836–8852.

(56) Wasserman, E.; Hsi, E; Young, W. T. *Polym. Prepr.* **1998**, *39* (2), 425–426.

(57) Ferrero, M. A.; Chiovetta, M. G. *Polym. Eng. Sci.* **1991**, *31* (12), 904.